KJO
pISSN: 1011-8942 eISSN: 2092-9382

Korean J Ophthalmol 2018;32(5):376-381
https://doi.org/10.3341/kjo.2017.0123

Original Article

Posterior Vitreous Structures Evaluated by Swept-source Optical Coherence Tomography with En Face Imaging

Jun Woo Park, Joo Eun Lee, Kang Yeun Pak

Department of Ophthalmology, Haeundae Paik Hospital, Inje University College of Medicine, Busan, Korea

Purpose: To evaluate posterior vitreous structures using swept-source (SS) optical coherence tomography (OCT) with en face imaging.

Methods: We retrospectively reviewed OCT images of healthy individuals who did not have intra-ocular disease. We obtained high-definition horizontal and vertical line scans crossing the fovea and 3D scans using SS-OCT, with the 3D scan centered between the fovea and the optic-nerve head. An enhanced vitreous visualization function was used to highlight vitreous structures. En face mode was used to measure the area of Martegiani (AM) and bursa premacularis (BP). We performed all measurements using a built-in function of the viewing software.

Results: We enrolled 24 eyes from 12 healthy individuals. The mean patient age was 28.7 ± 4.6 years (range, 24 to 39 years). The mean AM and BP areas were 5.73 ± 0.88 and 18.76 ± 6.95 mm^2, respectively. In en face imaging, AM shape was most frequently a vertical oval (18 / 22, 81.8%), while the predominant BP shape was round (16 / 20, 80.0%). AM was in contact with the optic disc, either at the temporal-disc margin (13 eyes, 59.1%) or the nasal optic-disc margin (9 eyes, 40.9%).

Conclusions: Posterior vitreous structures, such as AM and BP, were readily visualized using en face imaging with SS-OCT. Investigating normal vitreous configuration might help in understanding changes in vitreous structures associated with retinal pathology.

Key Words: Area of Martegiani, Bursa premacularis, En face, Swept-source optical coherence tomography, Vitreous body

The vitreous body is gelatinous material that fills intra-ocular space [1,2] and is often associated with various ocular diseases. Anomalous posterior vitreous detachment (PVD) is associated with pathologic conditions, such as macular hole, vitreomacular traction syndrome, or epiretinal membrane [3,4]. However, little is known about the vitreous structure, largely because it is transparent. Most of the information about vitreous anatomy is based on postmortem pathologic studies [1,2]. With the development of optical coherence tomography (OCT), *in vivo* imaging of the posterior vitreous became possible. Many investigators confirmed the presence of two distinct empty spaces in the posterior vitreous body. One is the area of Martegiani (AM) at the posterior end of Cloquet's canal, which forms from

Received: October 23, 2017 *Accepted*: March 20, 2018

Corresponding Author: Kang Yeun Pak, MD. Department of Ophthalmology, Haeundae Paik Hospital, #875 Haeundae-ro, Haeundae-gu, Busan 48108, Korea. Tel: 82-51-797-2310, Fax: 82-51-797-2030, E-mail: pky0402@naver.com

the regressed hyaloid artery during fetal development and is located over the optic disc. The other is bursa premacularis (BP), which is also known as the posterior precortical vitreous pocket (PPVP) and is located above the macula [5-9]. The presence of BP has been confirmed by various methods, including Indian-ink injection in the postmortem eye [10], triamcinolone injection during vitrectomy [11], and, more recently, OCT [5-7].

In this study, we aimed to quantitatively and qualitatively analyze posterior vitreous structures in healthy adults using swept-source OCT (SS-OCT) with en face imaging.

Materials and Methods

This cross-sectional study was performed in Inje university Haeundae Paik Hospital in May 2016. We retrospectively reviewed OCT images from healthy individuals who had no history of intra-ocular disease. Exclusion criteria included myopia of more than -4 diopters or axial length more than 26 mm. If eligible, both eyes were analyzed. SS-OCT (DRI OCT-1 Atlantis; Topcon, Tokyo, Japan) was used to acquire images of the vitreous structures. This machine uses a 1,050-nm wavelength and has a 100,000-A can/second scan speed and 8-μm axial resolution. Informed consent was waived due to the retrospective nature of the study. Informed consent was waived due to the retrospective nature of the study. This study was approved by the institutional review board of Inje University Haeundae Paik Hospital (2017-11-001-002) and adhered to the tenets of the Declaration of Helsinki.

OCT acquisition protocol

Twelve-millimetre horizontal and vertical line scans centered at the fovea were obtained (Fig. 1A, 1B). A 12 × 9-mm 3D cube scan included the optic disc and fovea. En face images were generated using built-in software (Fig. 1C).

OCT analysis of the posterior vitreous

The enhanced vitreous visualization function, one of the Topcon OCT viewing software's built-in functions, was applied for better visualization of the posterior vitreous. By simply clicking on the enhanced vitreous visualization function, the contrast was adjusted to highlight vitreous structures (Fig. 1A, 1B). The thickness and width of BP were measured using horizontal scanning (Fig. 1A). BP thickness was measured at the fovea center. BP width was defined as the maximum diameter through the fovea and the disc in a horizontal scan. The cross-sectional shape of BP, as observed in a horizontal scan, was categorized into boat, wedge, or irregular shape (Fig. 2). BP was classified as a boat shape when it had a trapezoidal shape in which the upper border was longer than the lower border (Fig. 2A) and was classified as a wedge shape when it had a trapezoidal shape in which the lower border was longer than the upper border (Fig. 2B). When neither classification was applicable, BP was classified as having an irregular shape (Fig. 2C).

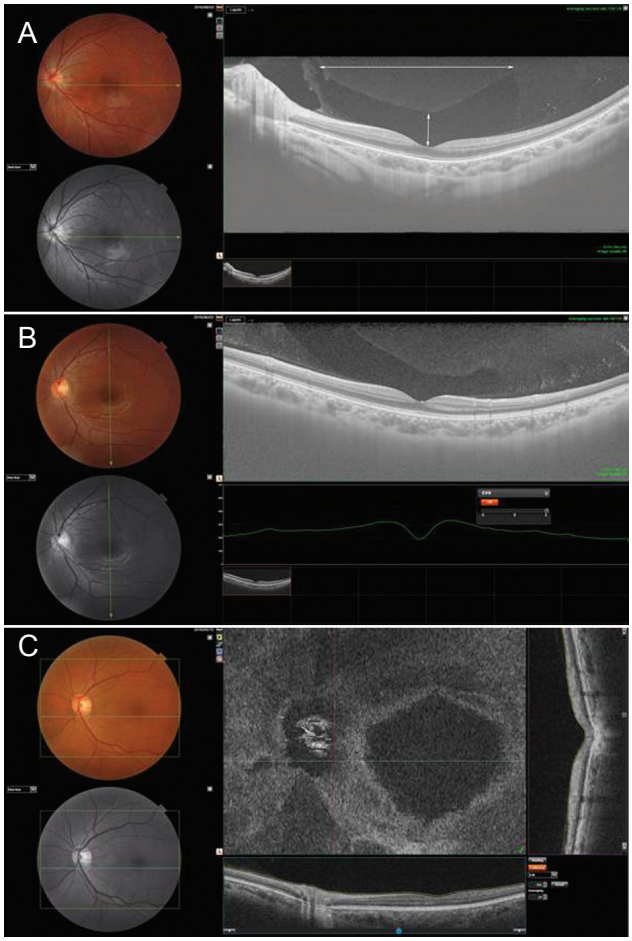

Fig. 1. (A) Twelve-millimetre horizontal line scan centered at the fovea: the enhanced vitreous visualization function was turned on, and the vitreous structure is highlighted. Horizontal and vertical arrows indicate width and central thickness of bursa premacularis, respectively. (B) Twelve-millimetre vertical line scan. (C) En face image generated from a 12 × 9-mm 3D cube scan.

Briefly, en face images that fit internal limiting membrane lines were generated and moved 20 to 40 μm anteriorly to the vitreous cavity to generate final images of AM and BP (Fig. 1C). The juxta-retinal area of AM and BP were measured using the intrinsic measurement function of the software. Optic disc area (DA) was measured to investigate the correlation between DA and AM. Two authors (JWP and JEL) who were blind to all clinical information independently evaluated the juxta-retinal shapes of AM and BP. The authors classified the shapes as round, horizontal-oval, vertical-oval, or irregular. Discrepancies between the two authors were resolved by consensus.

Statistical analysis

IBM SPSS ver. 22.0 (IBM Corp., Armonk, NY, USA) was used for statistical analysis. Measured values are presented as mean and standard deviation. Spearman's correlation analysis was performed to investigate the correlation between DA and AM.

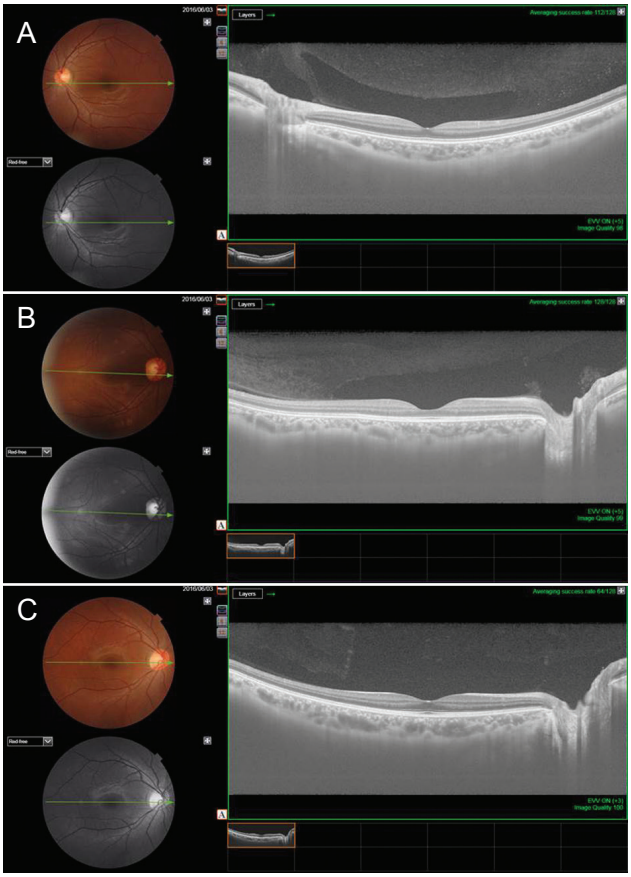

Fig. 2. Representative horizontal cross section images of bursa premacularis. (A) Boat shape, (B) wedge shape, and (C) irregular shape.

Results

Baseline characteristics

Twenty-four eyes of 12 healthy volunteers were included in this study. The mean patient age was 28.7 ± 4.61 years (range, 24 to 39; women, n=11). The mean refractive error was -0.97 ± 1.31 diopters, and the mean axial length was 24.66 ± 0.88 mm (Table 1).

Horizontal line scan measurements

BP was measurable in 16 eyes (66.67%) using horizontal line scans; it was not measurable in 8 eyes because it was hard to draw clear demarcation lines between BP and other vitreous structures. Mean thickness and BP width were 524.1 ± 96.8 μm (range, 318 to 674 μm) and 7,119.8 ± 999.5 μm (range, 5,716 to 8,737 μm), respectively. Boat shape was the predominant BP contour according to horizontal scans (11 / 16 eyes, 68.75%). Wedge shape was observed in 4 eyes (25%) and irregular shape in 1 eye (6.25%) (Fig. 2).

En face image measurements

AM and BP were measurable in 22 (91.67%) and 20 eyes (83.33%), respectively and not measurable in 2 and 4 eyes because of poor-quality images (Table 2). The juxta-retinal area of AM was 5.73 ± 0.88 mm^2 (range, 3.79 to 7.68 mm^2), while the juxta-retinal area of DA was 18.76 ± 6.95 mm^2 (range, 1.78 to 3.72 mm^2). The AM / DA ratio was 2.65 ± 0.53. There was no significant correlation between AM and

Table 1. Baseline patient characteristics

Characteristics	Value
No. of patients (eyes)	12 (24)
Mean age (yr)	28.7 ± 4.61 (24 to 39)
Sex (male : female)	1 : 11
Mean refractive error (diopters)	-0.97 ± 1.31 (-4.25 to +0.75)
Mean axial length (mm)	24.66 ± 0.88 (23.21 to 25.72)

Values are presented as number or mean ± standard deviation (range).

DA (p = 0.167) (Fig. 3). Most juxta-retinal AM areas were vertical-oval (18 / 22, 81.8%) followed by irregular shape (4 / 22, 18.2%). The BP juxta-retinal shape was mostly round (16 / 20, 80.0%), followed by horizontal-oval (2 / 20, 10.0%) and vertical-oval (2 / 20, 10.0%) (Table 2). Frequently, we observed that AM shared its border with the optic disc, either at the temporal or nasal margin: temporal-disc margin = 13 eyes (59.1%) (Fig. 4A), and nasal optic-disc margin = 9 eyes (40.9%) (Fig. 4B).

Discussion

Advances in OCT technology offer a new opportunity to study vitreous structures. Noninvasive imaging of posterior vitreous structures, such as AM and BP, became possible with the introduction of spectral domain OCT [6]. Although most of the commercially available spectral domain OCT machines are best employed to visualize retina structures, imaging of the choroid and vitreous is also possible

Table 2. Quantitative and qualitative analyses of the AM and BP in en face imaging

	AM	BP
Percent measurable	22 / 24 (91.67)	20 / 24 (83.33)
Mean area (mm^2)	5.73 ± 0.88 (3.79–7.68)	18.76 ± 6.95 (8.11–32.41)
AM / DA ratio	2.65 ± 0.53 (1.78–3.72)	NA
Shape		
Round	0	16 / 20 (80.0)
Horizontal oval	0	2 / 20 (10.0)
Vertical oval	18 / 22 (81.8)	2 / 20 (10.0)
Irregular	4 / 22 (18.2)	
Share of border		
Border at the temporal optic disc margin	13 / 22 (59.1)	NA
Border at the nasal optic disc margin	9 / 22 (40.9)	NA

Values are presented as number (%) or mean ± standard deviation (range).
AM = area of Martegiani; BP = bursa premacularis; DA = disc area; NA = not applicable.

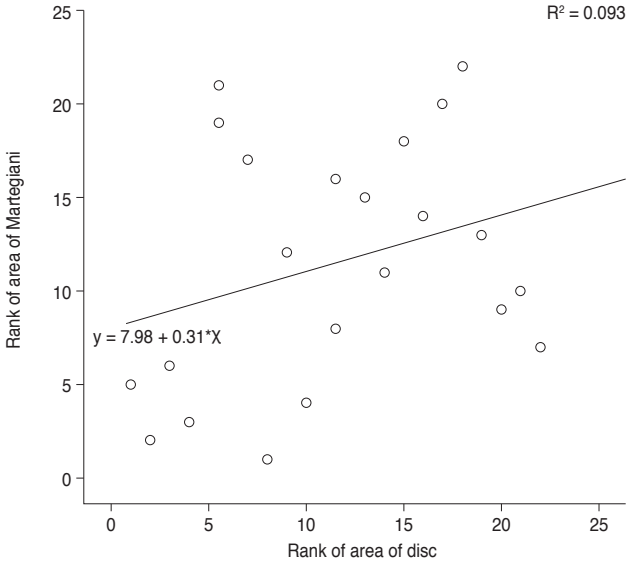

Fig. 3. Spearman correlation analysis of the optic disc area and the area of Martegiani.

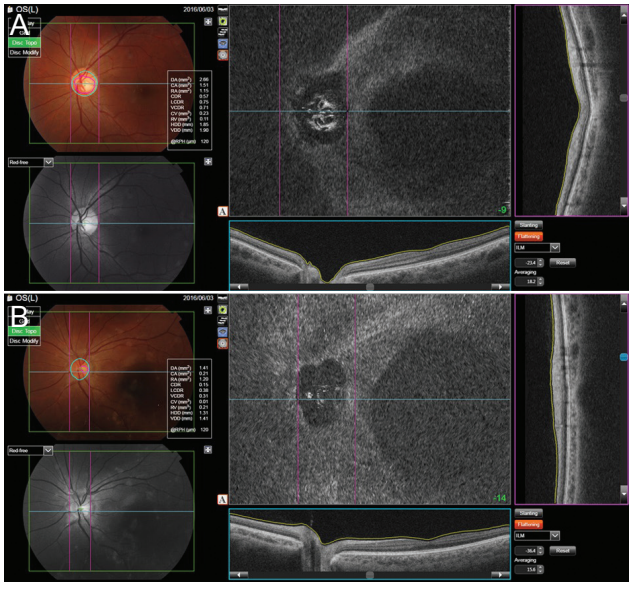

Fig. 4. Spatial relationship between optic disc margin and area of Martegiani (AM) margin. (A) The AM margin shares its temporal border with the optic disc. (B) The AM margin shares its nasal border with the optic disc.

using a modified scanning technique [6,8,12,13]. Moreover, high-quality vitreous images can be obtained without special SS-OCT measures, because of SS-OCT's longer wavelength, fast scanning speed, and easy software enhancement [5,14].

The BP dimensions that we measured in this study are similar to those from other studies. Using 12-mm horizontal SS-OCT scanning, Itakura et al. [5] found that BP in healthy adults had a mean height and width of 708.1 and 6,420.6 μm, respectively. They further observed that BP central height increased with myopic refractive errors, and that BP was connected to Cloquet's canal in 93.1% of the eyes. Park et al. [15] reported a mean BP height and width of 471.4 and 7,679 μm, respectively.

Our BP detection rate was 91.5% in eyes without PVD, 21% in eyes with partial PVD, and 0% in eyes with complete PVD, because posterior vitreous structures cannot be scanned because they move anteriorly with increased posterior vitreous detachment. Park and Oh [8] have shown that the proportion of temporal length to the entire horizontal diameter was significantly greater in adults than in children, and they found a positive correlation between age and proportion, suggesting progressive temporal extension of BP during childhood growth. BP and AM were connected in most cases, suggesting a direct anteroposterior connection between the retroretinal and premacular spaces [9]. However, none of these studies observed BP and AM using en face imaging.

Itakura et al. [14] showed that en face imaging, as well as horizontal scanning, of AM and BP can be obtained using SS-OCT. With horizontal scanning, they recorded a mean length and width of PPVPs of 6,546 and 5,795 μm, respectively, and a mean length and width of Cloquet's canals of 1,934 and 3,153 μm. However, they did not measure the areas of these two spaces using en face imaging. Furthermore, while they noted that the anterior PPVP in en face images indicated a crescent-shaped structure in all eyes, they did not discuss the general features of AM and BP. In this study, the most common shape observed using en face imaging was vertical-oval for AM and round for BP.

AM and BP are physiologically liquefied lacuna, anterior to the optic disc and macular area. Although the specific gravity of vitreous gel versus AM and BP contents is not well defined, it is thought that gravitational effects make oval and round shapes most common. Additionally, because BP is a space within the vitreous gel, its shape and anterior configuration might change in different situations. The superior BP is usually larger when the subject is seated, as in this study, and the anterior BP border is displaced more anteriorly when the subject is supine compared with seated [16]. The sizes of AM and BP were 5.73 ± 0.88 and 18.76 ± 6.95 mm^2, respectively. The AM was larger than the optic DA, with an AM/DA ratio of 2.65. Although we assumed that AM would correlate with DA, we did not find a statistically significant result. This may be due to the small number of enrolled eyes in this study. Furthermore, errors in the automatic DA-measurement function in the software would likely have a meaningful impact. One particularly interesting finding was that AM shared its border with the optic disc, either at the temporal or nasal margin, but the clinical implications of this observation require further elucidation.

Our study has several limitations. First, we enrolled a small number of participants, which negatively affected our ability to make comparisons across age groups. Second, the quality of en face images was poor for several participants. Improvements in OCT machines with respect to faster scanning speed, additional averaging, and fixation tracking are necessary for obtaining higher quality en face images of the vitreous. Further larger-scale studies, particularly those that include eyes with ocular diseases, will shed light on the role of posterior vitreous pockets in various vitreoretinal diseases.

In conclusion, en face images obtained with SS-OCT clearly showed the variable morphology of posterior vitreous structures, including AM and BP. The most common shapes observed in the en face images for AM and BP were vertical-oval and round, respectively. AM shares a border with the optic disc, either at the temporal or nasal margin. We investigated, *in vivo*, the posterior vitreous structure using OCT in normal participants. However, we could not compare structures in patients with various retinal diseases, which was a major limitation of the study. Nevertheless, investigating normal configurations of the vitreous could be useful in studying the changes in vitreous structures associated with retinal pathologies.

Conflict of Interest

No potential conflict of interest relevant to this article was reported.

References

1. Sebag J. Ageing of the vitreous. *Eye (Lond)* 1987;1:254-62.
2. Sebag J. Anatomy and pathology of the vitreo-retinal interface. *Eye (Lond)* 1992;6:541-52.
3. Duker JS, Kaiser PK, Binder S, et al. The International Vitreomacular Traction Study Group classification of vitreomacular adhesion, traction, and macular hole. *Ophthalmology* 2013;120:2611-9.
4. Sebag J. Anomalous posterior vitreous detachment: a unifying concept in vitreo-retinal disease. *Graefes Arch Clin Exp Ophthalmol* 2004;242:690-8.
5. Itakura H, Kishi S, Li D, Akiyama H. Observation of posterior precortical vitreous pocket using swept-source optical coherence tomography. *Invest Ophthalmol Vis Sci* 2013;54:3102-7.
6. Kim YC, Harasawa M, Salcedo-Villanueva G, et al. Enhanced high-density line spectral-domain optical coherence tomography imaging of the vitreoretinal interface: description of selected cases. *Semin Ophthalmol* 2016;31:559-66.
7. Liu JJ, Witkin AJ, Adhi M, et al. Enhanced vitreous imaging in healthy eyes using swept source optical coherence tomography. *PLoS One* 2014;9:e102950.
8. Park KA, Oh SY. Posterior precortical vitreous pocket in children. *Curr Eye Res* 2015;40:1034-9.
9. Schaal KB, Pang CE, Pozzoni MC, Engelbert M. The premacular bursa's shape revealed in vivo by swept-source optical coherence tomography. *Ophthalmology* 2014;121:1020-8.
10. Worst JG. Cisternal systems of the fully developed vitreous body in the young adult. *Trans Ophthalmol Soc U K* 1977;97:550-4.
11. Kishi S, Shimizu K. Posterior precortical vitreous pocket. *Arch Ophthalmol* 1990;108:979-82.
12. Spaide RF, Koizumi H, Pozzoni MC. Enhanced depth imaging spectral-domain optical coherence tomography. *Am J Ophthalmol* 2008;146:496-500.
13. Itakura H, Kishi S. Aging changes of vitreomacular interface. *Retina* 2011;31:1400-4.
14. Itakura H, Kishi S, Li D, Akiyama H. En face imaging of posterior precortical vitreous pockets using swept-source optical coherence tomography. *Invest Ophthalmol Vis Sci* 2015;56:2898-900.
15. Park SH, Lee JW, Lee MJ, et al. Evaluation of the cortical vitreous using swept-source optical coherence tomography in normal eyes. *J Korean Ophthalmol Soc* 2016;57:595-600.
16. Itakura H, Kishi S. Alterations of posterior precortical vitreous pockets with positional changes. *Retina* 2013;33:1417-20.